IEEE Access
Multidisciplinary | Rapid Review | Open Access Journal

Received April 4, 2019, accepted April 8, 2019, date of publication April 15, 2019, date of current version May 22, 2019.

*Digital Object Identifier 10.1109/ACCESS.2019.2911025*

# A Fusion Methodology to Bridge GPS Outages for INS/GPS Integrated Navigation System

**YUEXIN ZHANG**

Key Laboratory of Micro-Inertial Instrument and Advanced Navigation Technology, Ministry of Education, School of Instrument Science and Engineering, Southeast University, Nanjing 210096, China
Department of Electrical and Computer Engineering, National University of Singapore, Singapore 117576

e-mail: smileyuexin@163.com

This work was supported by the China Scholarship Council.

**ABSTRACT** The performance of an inertial navigation system (INS) and global positioning system (GPS) integrated navigation system is reduced during GPS outages. To bridge GPS outages, a fusion methodology to provide pseudo GPS position information is proposed. The methodology consists of two parts, empirical mode decomposition threshold filtering (EMDTF) and a long short-term memory (LSTM) neural network. The EMDTF eliminates the noise in inertial sensors and provides more accurate data for subsequent calculations. The LSTM uses the current specific forces and angular rates to predict the pseudo GPS position during GPS outages. To evaluate the effectiveness of the proposed methodology, numerical simulations and real field tests are employed. Compared with the traditional artificial neural networks, the results illustrate the proposed methodology can significantly improve the navigation accuracy during GPS outages and the model is simpler.

**INDEX TERMS** INS/GPS integrated navigation, empirical mode decomposition threshold filtering, long short-term memory neural network, GPS outages.

## I. INTRODUCTION

The integrated navigation system of inertial navigation system (INS) and global positioning system (GPS) has been widely used for vehicle applications [1]–[3]. However, GPS signals may not be available in certain environments, such as tunnels, forests and tall buildings [4], [5], so that the integrated navigation system INS/GPS works in pure INS mode. INS errors accumulate over time due to inertial measurement units (IMU) scale factor instability and bias error drift [6], [7], so the degradation of navigation performance is unavoidable during GPS outages.

Many methods have been presented to improve the INS/GPS integrated navigation system during GPS outages. One solution is to add auxiliary sensors such as odometer [8], [9], map data [10], wheel speed sensor and steering angle sensor [11] to provide external observations during GPS outages. This solution can achieve good navigation performance, but the cost and complexity of the navigation system will be increased. Another solution is based on time series prediction. Autoregressive model-based forward estimator [12] and grey predictor [13] are used to correct INS errors. These methods can quickly update parameters, but the effect of these methods is not obvious when GPS data are unavailable for a long time or vehicle mobility changes greatly. There are other solutions, such as the usage of other sensor systems (e.g., reduced inertial sensor system) to replace the INS in some applications [14], the usage of other nonlinear error modeling systems (e.g., particle filter) [15], [16]. In addition to the above solutions, the approaches based on artificial neural network (ANN) have been widely proposed to improve navigation performance, which can overcome the shortcoming of the second solution. The ANN-based methods include radial basis function neural network [17]–[19], multi-layer perceptron neural network [20], [21], and neuro-fuzzy inference system [22], [23]. The main idea of ANN-based approaches is to establish the internal relationship between IMU/INS outputs and GPS information. ANN models with different inputs and outputs have been researched. One of the models uses specific forces and angular rates of IMU as inputs of ANN model to predict the GPS position increments [24]. This model is simple, but the effect is limited. To achieve better prediction, velocity and/or attitude are also used as inputs [25]. In addition,

The associate editor coordinating the review of this manuscript and approving it for publication was Yunjie Yang.

different types of past data (e.g., past 1-step, past 10-steps) are added to the inputs [21]–[26]. However, these extra inputs will increase the complexity of model. Moreover, the above methods lack pre-filtering of IMU data to eliminate the noise of original measurement, which will affect the prediction effect of ANN.

To overcome the weakness of traditional ANN methods, a fusion method based on long short-term memory (LSTM) neural network is proposed. The LSTM network can adaptively use historical data without increasing the extra inputs, so it can achieve good prediction performance and keep the model simple. Meanwhile, a data preprocessing approach based on empirical mode decomposition threshold filtering (EMDTF) is presented to eliminate noise in IMU data. The proposed methodology is applied in INS/GPS integrated navigation system. The effectiveness of the proposed methodology is verified by numerical simulations and real road tests. The results show that navigation accuracy are significantly improved compared with traditional ANN-based methods.

The structure of this paper is as follows: The mathematical model is introduced in Section 2. Section 3 presents the data preprocessing algorithm and LSTM neural network in detail. In Section 4, numerical simulations and real road tests are carried out and analyzed. Section 5 is devoted to the conclusions.

## II. MATHEMATICAL MODEL

### A. INS ERROR MODEL

The INS is the essential sensor whether in training mode or prediction mode, providing attitude, position and velocity information. The navigation frame (n-frame) uses east-north-upward geographic coordinate system, and the body frame (b-frame) uses the right-forward-upward coordinate system. The INS error equations are derived in details in references [27], [28].

The INS attitude error equation is:

$$\dot{\boldsymbol{\psi}}^n = \delta\boldsymbol{\omega}_{ie}^n + \delta\boldsymbol{\omega}_{en}^n - \left(\boldsymbol{\omega}_{ie}^n + \boldsymbol{\omega}_{en}^n\right) \times \boldsymbol{\psi}^n - \boldsymbol{\varepsilon}^n \tag{1}$$

where $\boldsymbol{\psi}^n = [\psi_E, \psi_N, \psi_U]^T$ is attitude angle error vector in n-frame, $\psi_E$ denotes the pitch angle error, $\psi_N$ represents the roll angle error, and $\psi_U$ means the yaw angle error; $\boldsymbol{w}_{ie}^n$ and $\delta\boldsymbol{w}_{ie}^n$ are the rotating angular velocity caused by the earth's rotation and its error; $\boldsymbol{w}_{en}^n$ and $\delta\boldsymbol{w}_{en}^n$ are the angular velocity of the rotation of a navigation coordinate frame relative to earth and its error; $\boldsymbol{\varepsilon}^n$ is the gyroscopes' drift vector onto the n-frame.

The INS velocity error equation is:

$$\delta\dot{\boldsymbol{V}}^n = \boldsymbol{f}^n \times \boldsymbol{\psi}^n - \left(2\delta\boldsymbol{\omega}_{ie}^n + \delta\boldsymbol{\omega}_{en}^n\right) \times \boldsymbol{V}^n - \left(2\boldsymbol{\omega}_{ie}^n + \boldsymbol{\omega}_{en}^n\right) \times \delta\boldsymbol{V}^n + \boldsymbol{\nabla}^n \tag{2}$$

where $\delta\boldsymbol{V}^n = [\delta V_E, \delta V_N, \delta V_U]^T$ is the velocity error vector, $\delta V_E$ denotes the east velocity error, $\delta V_N$represents the north velocity error, and $\delta V_U$ means the upward velocity error; $\boldsymbol{f}^n$ represents the specific force vector; $\boldsymbol{V}^n = [V_E, V_N, V_U]^T$ is the velocity vector, $V_E$ denotes the east velocity, $V_N$ represents the north velocity, and $V_U$ means the upward velocity; $\boldsymbol{\nabla}^n$ represents the accelerometers' bias onto the n-frame.

The equations of INS position error are given by:

$$\begin{cases} \delta\dot{L} = \dfrac{1}{R_M + h}\delta V_N - \dfrac{V_N}{(R_M + h)^2}\delta h \\ \delta\dot{\lambda} = \dfrac{\sec L}{R_N + h}\delta V_E + \dfrac{V_E}{R_N + h}\sec L \cdot \tan L \cdot \delta L \\ \qquad\qquad - \dfrac{V_E \sec L}{(R_N + h)^2}\delta h \\ \delta\dot{h} = \delta V_U \end{cases} \tag{3}$$

where $L$, $\lambda$ and $h$ represent latitude, longitude and height, respectively; $\delta L$, $\delta\lambda$ and $\delta h$ denote their corresponding errors; $R_N$ and $R_M$ are the radii of the curvatures in meridian and prime vertical, respectively.

### B. KALMAN FILTER

Ignoring the effect of some small quantities, the INS error model suitable for vehicle stop and motion can be seen as a linear system, so the Kalman filter (KF) can be used to correct the INS errors [19], [29]–[30].

Taking into account the accuracy and real-time, the system uses a 15-dimensional state vector. The state vector $\boldsymbol{X}$ is given by:

$$\boldsymbol{X} = [\psi_E, \psi_N, \psi_U, \delta V_E, \delta V_N, \delta V_U, \delta L, \delta\lambda, \delta h, \nabla_{bx}, \nabla_{by}, \nabla_{bz}, \varepsilon_{bx}, \varepsilon_{by}, \varepsilon_{bz}]^T \tag{4}$$

where $\nabla_{bx}$, $\nabla_{by}$ and $\nabla_{bz}$ are three accelerometers' biases in b-frame, respectively; $\varepsilon_{bx}$, $\varepsilon_{by}$ and $\varepsilon_{bz}$ are three gyroscopes' drifts in b-frame, respectively.

Based on the INS error model, the discrete state space equations can be given by:

$$\begin{cases} \boldsymbol{X}_k = \boldsymbol{F}_{k,k-1}\boldsymbol{X}_{k-1} + \boldsymbol{G}_k\boldsymbol{W}_k \\ \boldsymbol{Z}_k = \boldsymbol{H}_k\boldsymbol{X}_k + \boldsymbol{V}_k \end{cases} \tag{5}$$

where $\boldsymbol{F}_{k,k-1}$ represents the state transition matrix; $\boldsymbol{G}_k$ denotes the system noise distribution matrix; $\boldsymbol{W}_k$ and $\boldsymbol{V}_k$ are process noise and measurement noise; $\boldsymbol{H}_k$is the measurement matrix; $\boldsymbol{Z}_k$ is the measurement vector.

The time prediction equations of KF are given by:

$$\hat{\boldsymbol{X}}_{k,k-1} = \boldsymbol{F}_{k,k-1}\boldsymbol{X}_{k-1} \tag{6}$$

$$\boldsymbol{P}_{k,k-1} = \boldsymbol{F}_{k,k-1}\boldsymbol{P}_{k-1}\boldsymbol{F}_{k,k-1}^T + \boldsymbol{Q}_{k-1} \tag{7}$$

where $\hat{\boldsymbol{X}}_{k,k-1}$ represents a priori estimate value of state vector; $\boldsymbol{P}_{k,k-1}$ is a priori estimate error covariance matrix; $\boldsymbol{P}_{k-1}$ represents a posteriori estimate error covariance matrix; $\boldsymbol{Q}_{k-1}$ is the process noise covariance matrix.

The measurement update equations are expressed as:

$$\boldsymbol{K}_k = \boldsymbol{P}_{k,k-1}\boldsymbol{H}_k^T\left[\boldsymbol{H}_k\boldsymbol{P}_{k,k-1}\boldsymbol{H}_k^T + \boldsymbol{R}_k\right]^{-1} \tag{8}$$

$$\hat{\boldsymbol{X}}_k = \hat{\boldsymbol{X}}_{k,k-1} + \boldsymbol{K}_k\left(\boldsymbol{Z}_k - \boldsymbol{H}_k\hat{\boldsymbol{X}}_{k,k-1}\right) \tag{9}$$

$$\boldsymbol{P}_k = \boldsymbol{P}_{k,k-1} - \boldsymbol{K}_k\boldsymbol{H}_k^T\boldsymbol{P}_{k,k-1} \tag{10}$$

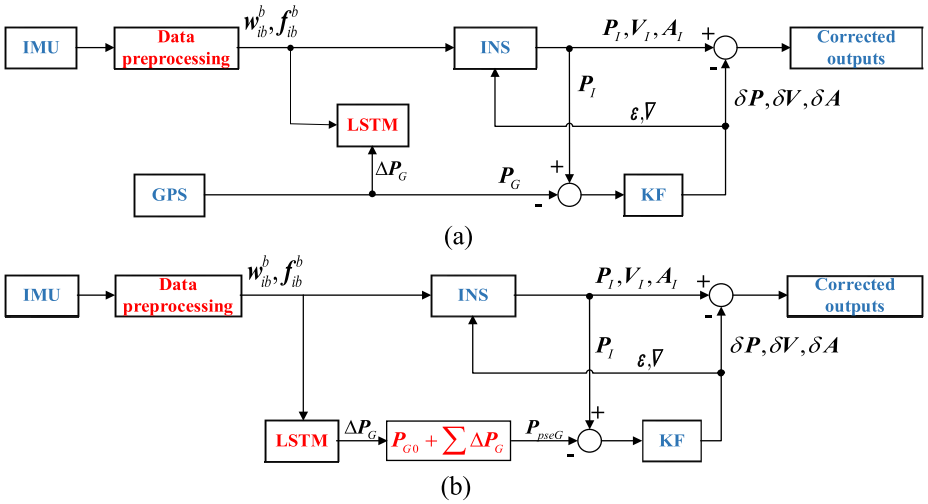


**FIGURE 1.** Proposed system structures. (a) Training mode. (b) Prediction mode.

where $\boldsymbol{K}_k$ denotes the Kalman gain matrix; $\hat{\boldsymbol{X}}_k$ represents a posteriori estimate value of state vector; $\boldsymbol{R}_k$ means the measurement error covariance matrix. The KF equations are derived in details in the reference [31].

## III. DESIGN OF THE NOVEL FUSION METHODOLOGY

To achieve high precision and continuous navigation information, the fusion methodology contains two parts, data preprocessing algorithm and long short-term memory neural network. The data preprocessing algorithm eliminates the noise of IMU data, providing more accurate data for subsequent calculations. The LSTM can accurately predict the pseudo GPS position during GPS outages and the model is simple.

### A. INTEGRATED SYSTEM SCHEME

The INS/GPS integrated navigation system adopts loosely-coupled combination mode, and the fusion method incorporating data preprocessing algorithm and LSTM is proposed in the system, as shown in Figure 1.

When GPS signals are available, the system operates in training mode, as shown in Figure 1(a). The position $\boldsymbol{P}_I$, velocity $\boldsymbol{V}_I$ and attitude $\boldsymbol{A}_I$ offered by INS and position $\boldsymbol{P}_G$ provided by GPS are integrated into KF. The estimated position error $\delta\boldsymbol{P}$, attitude error $\delta\boldsymbol{A}$ and velocity error $\delta\boldsymbol{V}$ are used to correct the navigation results of INS. The data preprocessing algorithm based on EMDTF is used to eliminate the noise in IMU data. Meanwhile, the LSTM module is trained, whose inputs are the current angular rate $\boldsymbol{w}_{ib}^b$ and specific force $\boldsymbol{f}_{ib}^b$, while the output is GPS position increment $\Delta\boldsymbol{P}_G$.

Once GPS signals are unavailable, the system works in prediction mode, as shown in Figure 1(b). The current angular rate $\boldsymbol{w}_{ib}^b$ and specific force $\boldsymbol{f}_{ib}^b$ are provided as inputs to LSTM, and the output of LSTM is the predicted GPS position increment $\Delta\boldsymbol{P}_G$. The predicted value $\Delta\boldsymbol{P}_G$ can be accumulated with initial position information $\boldsymbol{P}_{G0}$ to get pseudo-GPS position $\boldsymbol{P}_{pseG}$, which is then used to limit the divergence of inertial navigation error.

### B. DATA PREPROCESSING ALGORITHM

The data preprocessing algorithm combines the advantages of empirical mode decomposition (EMD) and wavelet threshold filtering, which can eliminate noise from IMU signal and retain useful signal as much as possible. First, the EMD adaptively decomposes the noisy IMU signal into a series of intrinsic mode functions (IMFs) according to amplitude and frequency. It overcomes the shortcomings of the fixed base function of wavelet transform and has a strong local adaptive. Then, the wavelet threshold filtering is applied to high-frequency IMFs, which separates the useful information in the high-frequency IMFs. How to select the threshold value and threshold function is the key to the wavelet threshold filtering. By comparing the effect of different methods to deal with IMU signal, heuristic threshold and soft threshold function are applied in this paper. Finally, these IMFs are added with IMFs of low frequency and residual signal to achieve de-noising signal. Figure 2 is the flowchart of IMU signal de-noising algorithm.

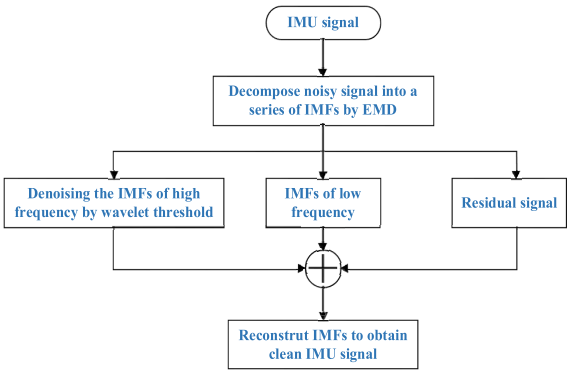


**FIGURE 2.** The flowchart of IMU signal de-noising.

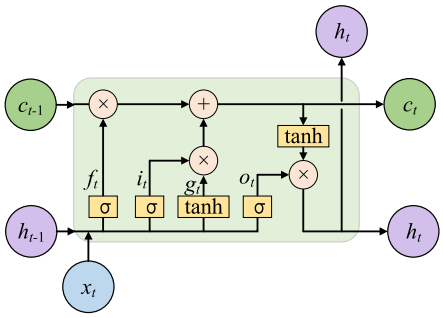


**FIGURE 3.** The structure of LSTM neural network.

### C. LONG SHORT-TERM MEMORY NEURAL NETWORK

The traditional neural networks cannot adaptively use the previous data. To achieve information persistence, the LSTM neural network is used in this paper. The LSTM is a special type of recurrent neural network (RNN), and has been wildly used in many fields (e.g. financial market prediction [32], wind speed forecasting [33], sentiment classification [34], voice detection [35]). Considering the advantages of LSTM, the LSTM is firstly proposed to forecast pseudo GPS position when GPS signals are unavailable, which establishes the relationship between the outputs of IMU and the GPS position increments. The inputs of LSTM are six parameters, while the inputs of traditional ANN (i.e. the model in reference [21]) are eighteen parameters.

The memory cell is the core component, and it consists of input gate (i.e., it determines if the input data will be used), forget gate (i.e., it decides if the last state will be forgotten) and output gate (i.e., it calculates if the information will be propagated). Figure 3 shows the structure of LSTM network.

The forward pass equations of LSTM are given by:

$$\begin{pmatrix} f_t \\ i_t \\ o_t \\ g_t \end{pmatrix} = \begin{pmatrix} \sigma \\ \sigma \\ \sigma \\ \tanh \end{pmatrix} \boldsymbol{W} \begin{pmatrix} h_{t-1} \\ x_t \end{pmatrix} \tag{11}$$

$$c_t = = f_t \odot c_{t-1} + i_t \odot g_t \tag{12}$$

$$h_t = o_t \odot \tanh(c_t) \tag{13}$$

where $x_t$ denotes the input data at time step $t$, $h_t$ denotes the hidden (output) state; functions $\sigma$ and tanh are applied element-wise; $i_t$ denotes input gate, $f_t$ represents forget gate, $o_t$ means output gate, and $g_t$ is used to modify the cell state $c_t$; $\boldsymbol{W}$ is corresponding weights matrix; $\odot$ represents the Hadamard product.

The above LSTM can forecast pseudo GPS position when GPS signals are unavailable. The prediction procedures are as follows.

Firstly, the LSTM neural network is trained. The inputs are the current angular rate $\boldsymbol{w}_{ib}^{b}$ and specific force $\boldsymbol{f}_{ib}^{b}$, and the output is GPS position increment $\Delta \boldsymbol{P}_G$. Secondly, the trained LSTM neural network is used to predict $\Delta \boldsymbol{P}_G$. The inputs are the same as the first procedure. Lastly, the predicted value $\Delta \boldsymbol{P}_G$ is accumulated with initial position information $\boldsymbol{P}_{G0}$ to get pseudo-GPS position $\boldsymbol{P}_{pseG}$.

**TABLE 1.** Sensors' specifications.

| Sensors | Parameters | Accuracy |
|---|---|---|
| IMU | Gyroscope bias stability in-run | $1^\circ/\text{hr}$ |
| | Gyroscope angular random walk | $0.0667^\circ/\sqrt{\text{hr}}$ |
| | Accelerometer bias stability in-run | 0.25mg |
| | Accelerometer velocity random walk | $55\mu\text{g}/\sqrt{\text{Hz}}$ |
| | Frequency | 100 Hz |
| GPS | Position | 1 m |
| | Frequency | 1 Hz |

**TABLE 2.** Motion states of the vehicle.

| Motion states | Time (s) |
|---|---|
| Acceleration | 0~10, 375~380, 795~800, 1165~1170, 1470~1475 |
| Uniform | 10~310, 380~730, 800~1100, 1170~1405, 1475~1790 |
| Deceleration | 310~315, 730~735, 1100~1105, 1405~1410, 1790~1800 |
| Left turning | 315~375, 1105~1165 |
| Right turning | 735~795, 1410~1470 |

## IV. PERFORMANCE EVALUATION

### A. NUMERICAL SIMULATIONS

To verify the proposed methodology, numerical simulations are performed. The specifications of sensors are shown in Table 1. The vehicle movements are various, and its detailed motion states are shown in Table 2.

To validate the data preprocessing algorithm proposed in section III comparative simulations of de-noising algorithm or not are carried out under the mode that GPS signals are available. During this simulation, EMD decomposes the IMUs signals. Then, the high-frequency $\text{IMF}_1$ and $\text{IMF}_2$ are preprocessed by wavelet threshold filtering. Finally, these IMFs are added with IMFs of low frequency and residual signal to achieve de-noising signals. Since the vehicle is assumed to move only in the horizontal plane, the errors of directions of east and north are shown in the paper. Figure 4 and Figure 5 depict the velocity and position errors, respectively. Table 3 evaluates the de-noising algorithm.

From Figures 4 and 5, it is obvious found that by using the data preprocessing algorithm, the accuracy of velocity and position have been significantly improved. As shown

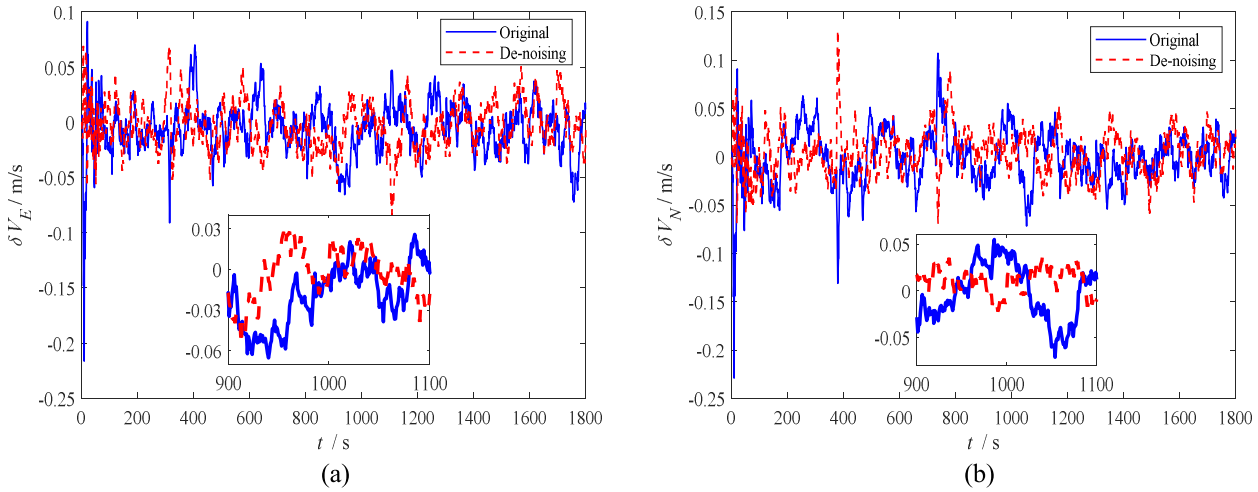


**FIGURE 4.** The velocity errors of de-noising algorithm. (a) East velocity error. (b) North velocity error.

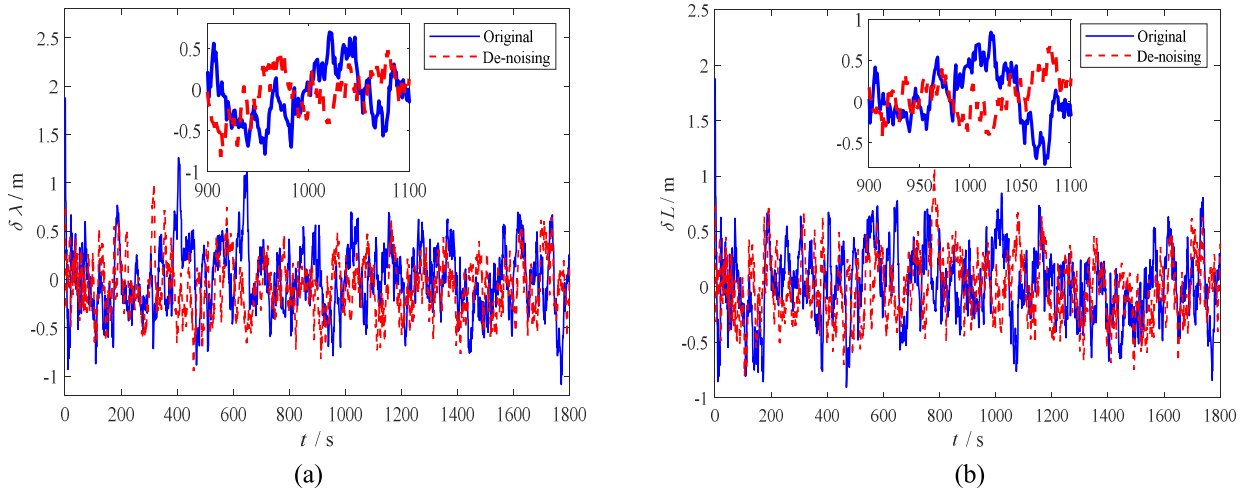


**FIGURE 5.** The position errors of de-noising algorithm. (a) Longitude error. (b) Latitude error.

**TABLE 3.** Evaluation of de-noising algorithm.

| Error | Original | | De-noising | |
|---|---|---|---|---|
| | Max | RMSE | Max | RMSE |
| East velocity (m/s) | 0.2161 | 0.0238 | 0.0837 | 0.0216 |
| North velocity (m/s) | 0.2288 | 0.0280 | 0.1313 | 0.0238 |
| Longitude (m) | 1.8825 | 0.3489 | 0.9939 | 0.3008 |
| Latitude (m) | 1.8824 | 0.3223 | 1.0684 | 0.2877 |

in Table 3, the max errors of the original algorithm for east velocity, north velocity, longitude and latitude are 0.2161m/s, 0.2288 m/s, 1.8825 m and 1.8824 m, respectively. After processing by the de-noising algorithm EMDTF, the max errors of the corresponding components are reduced to 0.0837 m/s, 0.1313 m/s, 0.9939 m and 1.0684 m, respectively. The improvement rates are about 61.28%, 42.61%, 47.2% and 43.24%, respectively. The corresponding root mean square error (RMSE) values are reduced by about 9.12%, 15.14%, 13.78% and 10.72%, respectively. The above results indicate

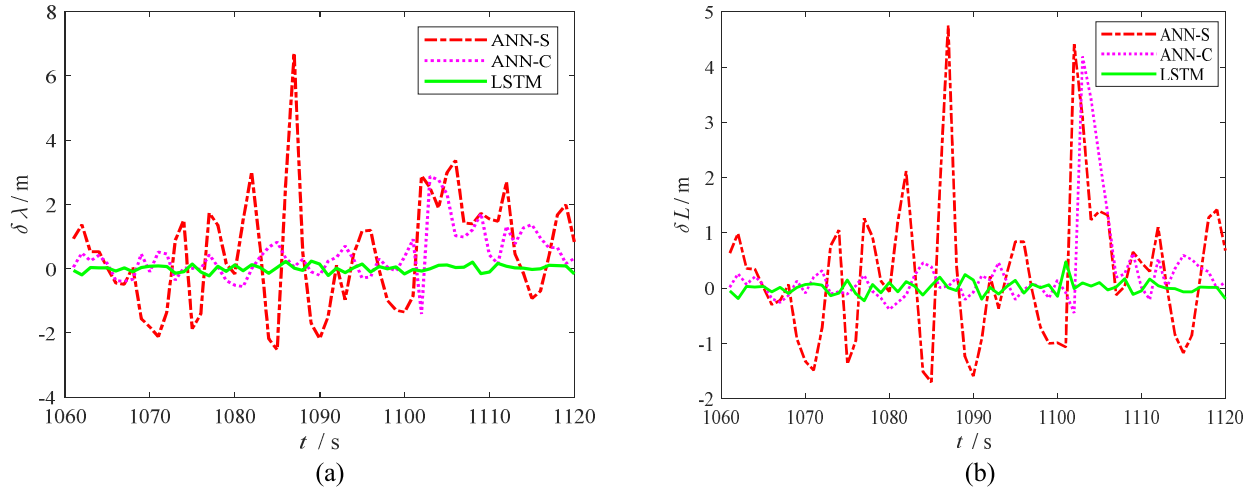


**FIGURE 6.** The prediction errors of position increments during 60 s GPS outages. (a) The prediction errors of longitude increment. (b) The prediction errors of latitude increment.

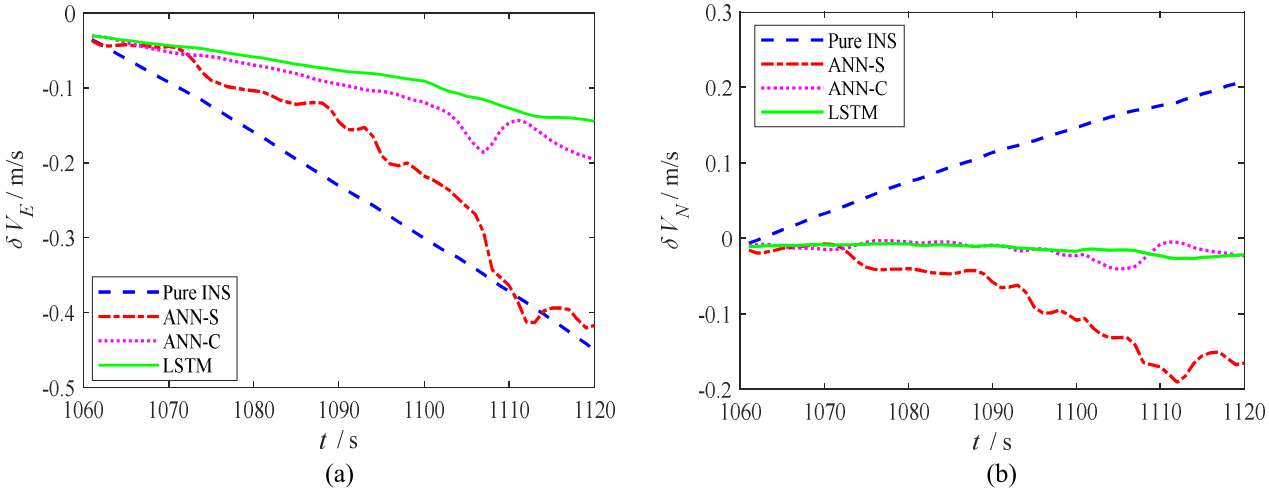


**FIGURE 7.** The velocity errors during 60 s GPS outages. (a) East velocity error. (b) North velocity error.

that the de-noising method is effective and can provide accurate IMU data for the following calculations.

To testify the validity of LSTM method, numerical simulations are performed by four methods: (1) pure INS (i.e., KF only executes time update process); (2) traditional artificial neural network with simple inputs (i.e., the inputs of ANN are current angular rate $\boldsymbol{w}_{ib}^{b}$ and specific force $\boldsymbol{f}_{ib}^{b}$); (3) traditional artificial neural network with complicated inputs [21] (i.e., the inputs of ANN are current and past 1-step angular rate $\boldsymbol{w}_{ib}^{b}$, specific force $\boldsymbol{f}_{ib}^{b}$ and velocity $\boldsymbol{V}_{I}$); (4) LSTM neural network with simple inputs (i.e., the inputs of LSTM are current angular rate $\boldsymbol{w}_{ib}^{b}$ and specific force $\boldsymbol{f}_{ib}^{b}$).

The system firstly works in the training mode, then we assume that the GPS signals are unavailable during the period of 1060 $\sim$ 1120 s, and the system works in the prediction mode. It is worth mentioning that the more abundant the training samples, the more accurate the training model, and then it can predict accurately. Figure 6 is the prediction errors of position increments (i.e., $\Delta \boldsymbol{P}_{G}$is Section 3.1) using different solutions. The RMSE values of longitude increment using simple ANN, complicated ANN and LSTM are 1.7795 m, 0.8539 m, and 0.1092 m, respectively. The RMSE values of latitude increment are 1.3186 m, 0.8191 m, and 0.1182 m, respectively. The results indicate that LSTM method can better establish inputs-outputs model and predict position increments more accurately than traditional ANNs.

Figure 7 and Figure 8 present velocity and position errors of the four solutions during 60 s GPS outages, respectively, and Table 4 summarizes the corresponding maximum errors and RMSE values.

To verify the effect of the proposed method under different movement states and outage time, another GPS outage is simulated. We assume that the GPS signal is unavailable during the period of 1600 $\sim$ 1700 s. Figure 9 and Figure 10 illustrate

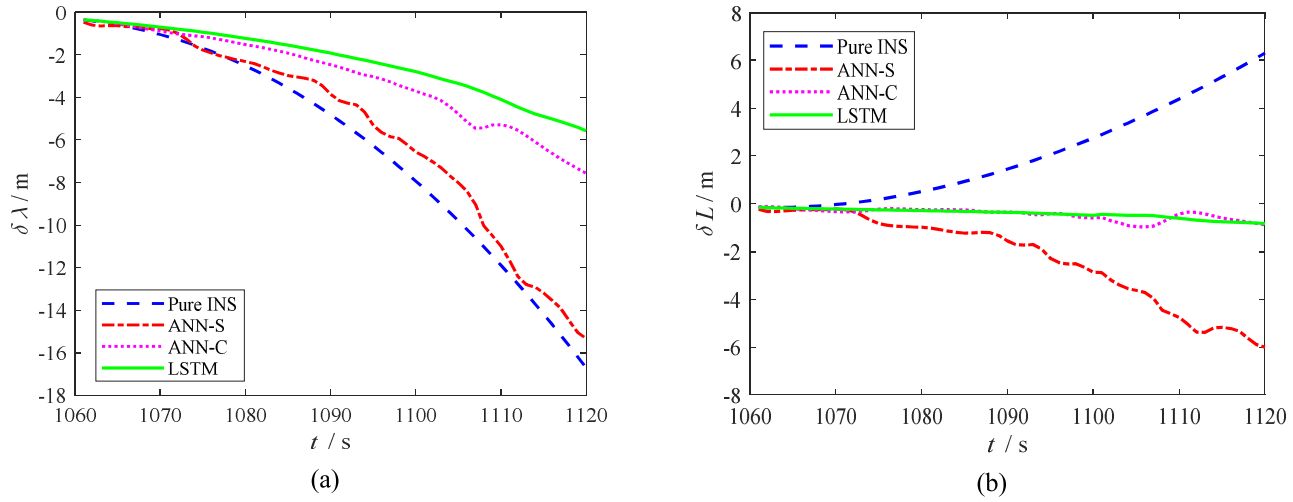


**FIGURE 8.** The position errors during 60 s GPS outages. (a) Longitude error. (b) Latitude error.

**TABLE 4.** The error statistics of different solutions during 60 s GPS outages.

| Error | Pure INS | | ANN-S | | ANN-C | | LSTM | |
|---|---|---|---|---|---|---|---|---|
| | Max | RMSE | Max | RMSE | Max | RMSE | Max | RMSE |
| East velocity (m/s) | 0.4504 | 0.2651 | 0.4208 | 0.2255 | 0.1959 | 0.1141 | 0.1451 | 0.0895 |
| North velocity (m/s) | 0.2090 | 0.1257 | 0.1905 | 0.0989 | 0.0405 | 0.0171 | 0.0268 | 0.0149 |
| Longitude (m) | 16.7193 | 7.8944 | 15.3449 | 7.0890 | 7.5638 | 3.6806 | 5.5627 | 2.7723 |
| Latitude (m) | 6.3116 | 2.8567 | 6.0048 | 2.8394 | 0.9704 | 0.4926 | 0.8285 | 0.4507 |

**TABLE 5.** The error statistics of different solutions during 100 s GPS outages.

| Error | Pure INS | | ANN-S | | ANN-C | | LSTM | |
|---|---|---|---|---|---|---|---|---|
| | Max | RMSE | Max | RMSE | Max | RMSE | Max | RMSE |
| East velocity (m/s) | 0.8167 | 0.4756 | 0.3116 | 0.1874 | 0.0427 | 0.0261 | 0.0152 | 0.0099 |
| North velocity (m/s) | 0.3368 | 0.1941 | 0.2643 | 0.1590 | 0.0513 | 0.0395 | 0.0314 | 0.0233 |
| Longitude (m) | 48.1652 | 21.7743 | 19.7460 | 9.5534 | 2.6613 | 1.3082 | 0.7235 | 0.3985 |
| Latitude (m) | 16.8037 | 7.6073 | 14.0163 | 6.6434 | 3.7417 | 2.1342 | 2.2393 | 1.2406 |

velocity and position errors of the four solutions during 100 s GPS outages, respectively, and Table 5 summarizes the corresponding maximum errors and RMSE values. The results show that the LSTM method has the best navigation accuracy. Compared with complicated ANN, the maximum errors of velocity and position errors are decreased by 64.40%, 38.79%, 72.81% and 40.15%; the RMSE values are decreased by 62.07%, 41.02%, 69.54% and 41.87%. In addition, the inputs of LSTM are much less than that of complicated ANN. It is worth mentioning that the positioning errors during GPS outages can be affected by the movement states of the vehicle. As the movement state of outage-100s is simpler than that of outage-60s, the positioning errors of outage-100s are lower than that of outage-60s.

From Figures 7-10 and Tables 4-5, it can found that four solutions show significantly different navigation accuracy: (1) pure INS performs the worst in these methods. For example, the maximum errors of position for second outage reach 48.1652 m and 16.8037 m. It can be attributed to the fact that the navigation accuracy decreases over time due to the inherent errors of IMU; (2) simple ANN performs better than the pure INS. The inputs of the model are current angular rates and specific forces, so this model is simple. Since the past useful information is not used, the effect of simple ANN

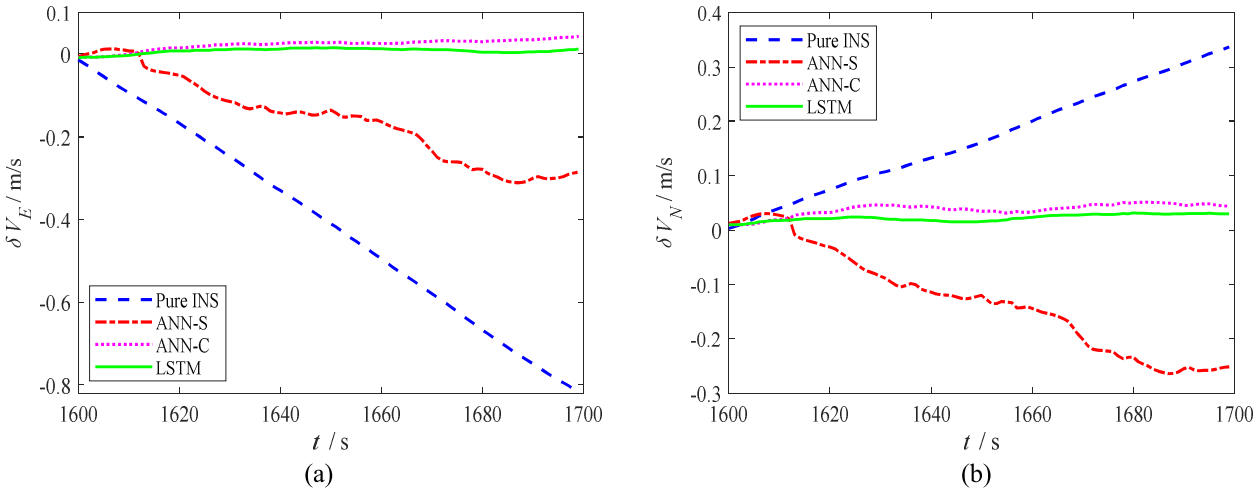


**FIGURE 9.** The velocity errors during 100 s GPS outages. (a) East velocity error. (b) North velocity error.

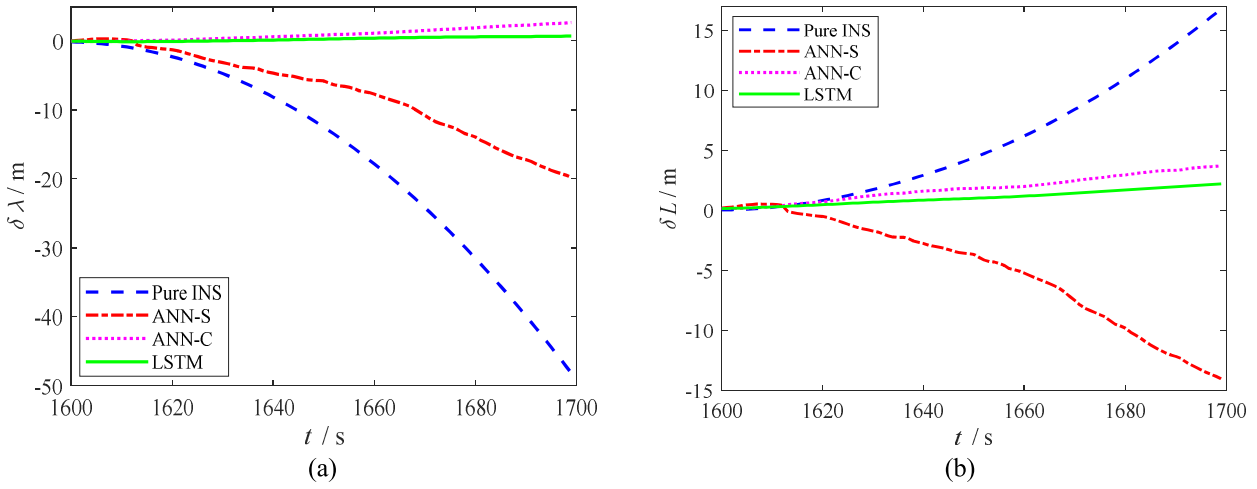


**FIGURE 10.** The position errors during 100 s GPS outages. (a) Longitude error. (b) Latitude error.

**TABLE 6.** Characteristics of ellipse-A IMUs.

| | Accelerometer | Gyroscope |
|---|---|---|
| Range | ±8g | ±450°/s |
| Gain stability | 1000ppm | 500ppm |
| Bias stability | ±5mg | ±0.2°/s |
| Random walk | $57\,\mathrm{ug}/\sqrt{\mathrm{Hz}}$ | $0.15°/\sqrt{\mathrm{hr}}$ |


**FIGURE 11.** Test vehicle with navigation system equipment.

is limited; (3) for the complicated ANN method, its navigation performance is greatly improved with respect to the simple ANN. For example, compared with the simple ANN, the RMSE values of longitude and latitude during 100 s GPS outages are decreased by 86.31% and 67.87%, respectively. Its inputs include present and past information of angular rates, specific forces and velocity. The algorithm is effective, but the model is more complicated; (4) the LSTM method has the best navigation accuracy. The RMSE values of longitude and latitude during 100 s GPS outages are decreased by

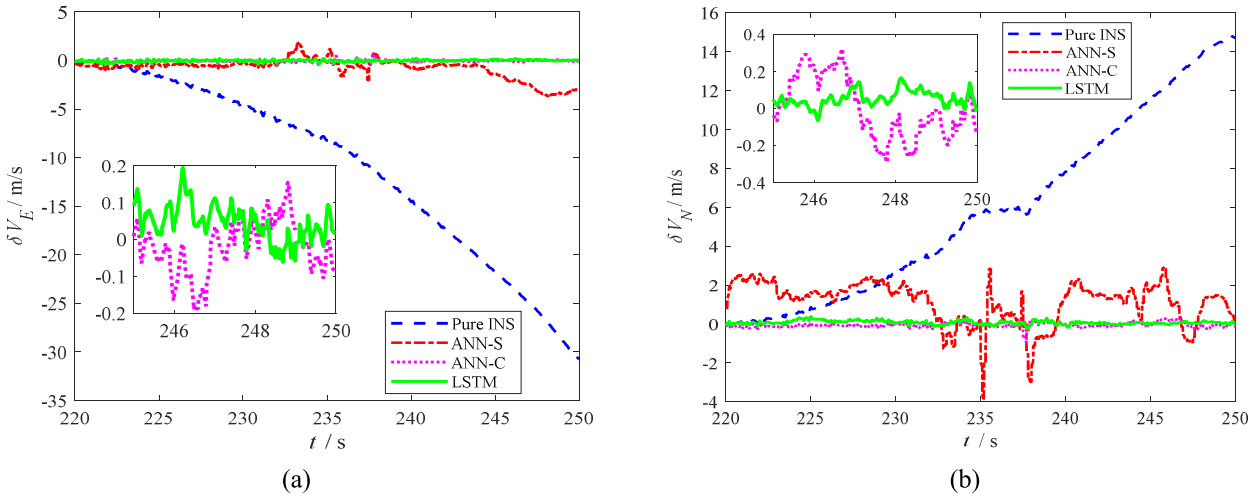


**FIGURE 12.** The velocity errors during 30 s GPS outages. (a) East velocity error. (b) North velocity error.

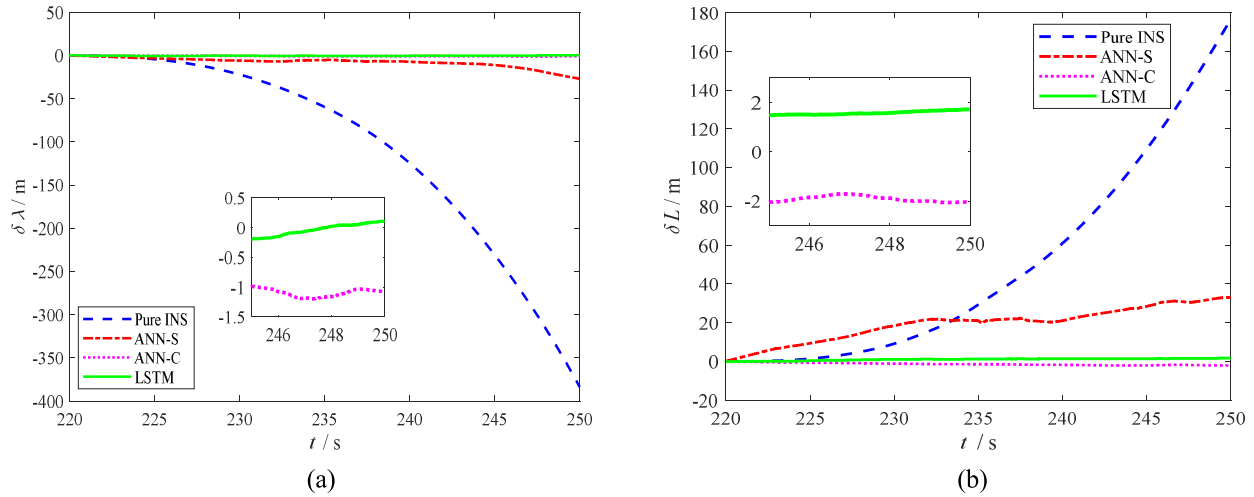


**FIGURE 13.** The position errors during 30 s GPS outages. (a) Longitude error. (b) Latitude error.

69.54% and 41.87%, respectively, with respect to complicated ANN. Moreover, the inputs of LSTM are much less than that of complicated ANN.

### B. REAL ROAD TESTS

To further validate the proposed approach, real road tests are performed. The IMU uses the Ellipse-A of SBG SYSTEMS Company, whose sampling frequency is set to 100Hz. The GPS receiver uses the Trimble Company, and the frequency is 1Hz. Real-time kinematic GPS provides high precision navigation, which is taken as the reference values. Figure 11 shows the test vehicle with navigation system equipment, and Table 6 lists the characteristics of Ellipse-A IMU.

To evaluate the performance of the proposed method, simulated GPS outage is intentionally introduced by artificially removing GPS solution. As the accuracy of IMU is low, the pure INS will rapidly diverge in a short time, so the real road test assumes that there is a GPS outage for a length of 30 s during the period 220∼250 s. It is worth mentioning that the IMU data used in following analysis are de-noising by the EMDTF. To maintain consistency with the simulations, the experimental tests are carried out on a road that is basically at the same height. Figure 12 and Figure 13 give the velocity and position errors, respectively. Table 7 summarizes the error statistics of four solutions.

Figures 12-13 and Table 7 show that four solutions have different effects: (1) pure INS has the largest errors. For example, the maximum errors of east and north velocity reach to 30.7543 m/s and 14.7981 m/s, respectively; (2) simple ANN performs better than the first method. The maximum errors of east and north velocity are reduced to 3.6994 m/s and 3.9464 m/s, respectively; (3) for the complicated ANN method, its navigation accuracy is increased by a level

**TABLE 7.** The error statistics of different solutions during 30 s GPS outages.

| Error | Pure INS | | ANN-S | | ANN-C | | LSTM | |
|---|---|---|---|---|---|---|---|---|
| | Max | RMSE | Max | RMSE | Max | RMSE | Max | RMSE |
| East velocity (m/s) | 30.7543 | 14.0810 | 3.6994 | 1.2868 | 0.6550 | 0.1322 | 0.4571 | 0.1034 |
| North velocity (m/s) | 14.7981 | 7.4694 | 3.9465 | 1.5532 | 0.9677 | 0.1374 | 0.3853 | 0.1170 |
| Longitude (m) | 383.7021 | 150.0310 | 26.9609 | 9.4836 | 1.2008 | 0.7500 | 0.5118 | 0.3373 |
| Latitude (m) | 176.5525 | 70.7885 | 33.0544 | 21.2713 | 2.0931 | 1.4562 | 1.7198 | 1.1699 |

compared with the simple ANN; (4) the LSTM method preforms best in the four solutions. The RMSE values of east velocity, north velocity, longitude and latitude are reduced by 21.79%, 14.85%, 55.03% and 19.66%, respectively, with respect to complicated ANN. Furthermore, the inputs of LSTM are six parameters while the inputs of the complicated ANN are eighteen parameters.

## V. CONCLUSIONS

A fusion method for INS/GPS integrated system during GPS outages is presented. It consists of de-noising algorithm and LSTM neural network. The de-noising algorithm based on EMDTF removes noise in IMU data and provides accurate data for subsequent calculations. The LSTM network is devised to predict the position increments. The main advantage is that the LSTM network not only uses the inputs of the current time, but also adaptively uses historical model information. To validate the effect of de-noising algorithm, comparative simulations are carried out. The results show that by using de-noising algorithm, the max errors of east velocity, north velocity, longitude and latitude are reduced by 61.28%, 42.61%, 47.2% and 43.24%, respectively. And the accuracy of the four components are improved by about 9.12%, 15.14%, 13.78% and 10.72%, respectively. To verify the performance of LSTM method, numerical simulations and real road tests are carried out. Compared with traditional complicated ANN method, the LSTM method reduces the RMSE values of east velocity, north velocity, longitude and latitude by 21.79%, 14.85%, 55.03% and 19.66%, respectively. Moreover, the model is simple. Therefore, the proposed method can effectively deal with GPS outages, thereby providing continuous high-precision navigation information for INS/GPS integrated navigation system in complex environments. Future work will concern the real-time implementation in applications.

## REFERENCES


[1] M. F. Abdel-Hafez, K. Saadeddin, and M. Jarrah, "Constrained low-cost GPS/INS filter with encoder bias estimation for ground vehicles' applications," *Mech. Syst. Signal Process.*, vols. 58–59, pp. 285–297, Jul. 2015.

[2] S. Godha and M. E. Cannon, "GPS/MEMS INS integrated system for navigation in urban areas," *GPS Solutions*, vol. 11, no. 3, pp. 193–203, Jul. 2007.

[3] A. D. Abosekeen and A. E. Abdalla, "Fusion of low-cost MEMS IMU/GPS integrated navigation system," in *Proc. 8th Int. Conf. Elect. Eng. (ICEENG)*, 2012, pp. EE213-1–EE213-17.

[4] M. Elazab, A. Noureldin, and H. S. Hassanein, "Integrated cooperative localization for vehicular networks with partial GPS access in urban canyons," *Veh. Commun.*, vol. 9, pp. 242–253, Jul. 2017.

[5] Z. Gao *et al.*, "Odometer, low-cost inertial sensors, and four-GNSS data to enhance PPP and attitude determination," *GPS Solutions*, vol. 22, no. 3, p. 57, 2018.

[6] S. Daneshmand and G. Lachapelle, "Integration of GNSS and INS with a phased array antenna," *GPS Solutions*, vol. 22, no. 1, p. 3, 2018.

[7] W. Wei, Z. Gao, S. Gao, and K. Jia, "A SINS/SRS/GNS autonomous integrated navigation system based on spectral redshift velocity measurements," *Sensors*, vol. 18, no. 4, p. 1145, 2018.

[8] M. Aftatah, A. Lahrech, and A. Abounada, "Fusion of GPS/INS/ odometer measurements for land vehicle navigation with GPS outage," in *Proc. Int. Conf. Cloud Comput. Technol. Appl.*, May 2018, pp. 48–55.

[9] J. Georgy, T. Karamat, U. Iqbal, and A. Noureldin, "Enhanced MEMS-IMU/odometer/GPS integration using mixture particle filter," *GPS Solutions*, vol. 15, no. 3, pp. 239–252, 2011.

[10] J. Georgy, A. Noureldin, and C. Goodall, "Vehicle navigator using a mixture particle filter for inertial sensors/odometer/map data/GPS integration," *IEEE Trans. Consum. Electron.*, vol. 58, no. 2, pp. 544–552, May 2012.

[11] Q. Xu, X. Li, and C.-Y. Chan, "Enhancing localization accuracy of MEMS-INS/GPS/in-vehicle sensors integration during GPS outages," *IEEE Trans. Instrum. Meas.*, vol. 67, no. 8, pp. 1966–1978, Aug. 2018.

[12] C. H. Lim, T. S. Lim, and V. C. Koo, "New GPS-aided SINU system modeling using an autoregressive model," *Int. J. Adv. Robotic Syst.*, vol. 12, no. 9, p. 121, 2015.

[13] X. Li and Q. Xu, "A reliable fusion positioning strategy for land vehicles in GPS-denied environments based on low-cost sensors," *IEEE Trans. Ind. Electron.*, vol. 64, no. 4, pp. 3205–3215, Apr. 2017.

[14] A. Abosekeen, A. Noureldin, and M. J. Korenberg, "Utilizing the ACC-FMCW radar for land vehicles navigation," in *Proc. IEEE/ION Position, Location Navigat. Symp. (PLANS)*, Apr. 2018, pp. 124–132.

[15] B. Cui, X. Chen, X. Yuan, H. Huang, and L. Xiao, "Performance analysis of improved iterated cubature Kalman filter and its application to GNSS/INS," *ISA Trans.*, vol. 66, pp. 460–468, Jan. 2017.

[16] J. Georgy, A. Noureldin, M. J. Korenberg, and M. M. Bayoumi, "Low-cost three-dimensional navigation solution for RISS/GPS integration using mixture particle filter," *IEEE Trans. Veh. Technol*, vol. 59, no. 2, pp. 599–615, Feb. 2010.

[17] L. Chen and J. Fang, "A hybrid prediction method for bridging GPS outages in high-precision POS application," *IEEE Trans. Instrum. Meas.*, vol. 63, no. 6, pp. 1656–1665, Jun. 2014.

[18] R. Sharaf and A. Noureldin, "Sensor integration for satellite-based vehicular navigation using neural networks," *IEEE Trans. Neural Netw.*, vol. 18, no. 2, pp. 589–594, Mar. 2007.

[19] L. Semeniuk and A. Noureldin, "Bridging GPS outages using neural network estimates of INS position and velocity errors," *Meas. Sci. Technol.*, vol. 17, no. 10, pp. 2783–2798, 2006.

[20] P. Aggarwal, D. Bhatt, V. Devabhaktuni, and P. Bhattacharya, "Dempster Shafer neural network algorithm for land vehicle navigation application," *Inf. Sci.*, vol. 253, pp. 26–33, Dec. 2013.

[21] Y. Yao, X. Xu, C. Zhu, and C.-Y. Chan, "A hybrid fusion algorithm for GPS/INS integration during GPS outages," *Measurement*, vol. 103, pp. 42–51, Jun. 2017.

[22] A. M. Hasan, K. Samsudin, and A. R. Ramli, "Optimizing of ANFIS for estimating INS error during GPS outages," *J. Chin. Inst. Eng.*, vol. 34, no. 7, pp. 967–982, 2011.

[23] V. Havyarimana, D. Hanyurwimfura, P. Nsengiyumva, and Z. Xiao, "A novel hybrid approach based-SRG model for vehicle position prediction in multi-GPS outage conditions," *Inf. Fusion*, vol. 41, pp. 1–8, May 2018.
[24] R. Sharaf, A. Noureldin, A. Osman, and N. El-Sheimy, "Online INS/GPS integration with a radial basis function neural network," *IEEE Aerosp. Electron. Syst. Mag.*, vol. 20, no. 3, pp. 8–14, Mar. 2005.
[25] J. Li, N. Song, G. Yang, M. Li, and Q. Cai, "Improving positioning accuracy of vehicular navigation system during GPS outages utilizing ensemble learning algorithm," *Inf. Fusion*, vol. 35, pp. 1–10, May 2017.
[26] X. Chen, C. Shen, W.-B. Zhang, M. Tomizuka, Y. Xu, and K. Chiu, "Novel hybrid of strong tracking Kalman filter and wavelet neural network for GPS/INS during GPS outages," *Measurement*, vol. 46, no. 10, pp. 3847–3854, Dec. 2013.
[27] D. Titterton and J. Weston, "Strapdown inertial navigation technology," *IEEE Aerosp. Electron. Syst. Mag.*, vol. 20, no. 7, pp. 33–34, Jul. 2004.
[28] Y. Liu, X. Fan, C. Lv, J. Wu, L. Li, and D. Ding, "An innovative information fusion method with adaptive Kalman filter for integrated INS/GPS navigation of autonomous vehicles," *Mech. Syst. Signal Process.*, vol. 100, pp. 605–616, Feb. 2018.
[29] D. Bhatt, P. Aggarwal, V. Devabhaktuni, and P. Bhattacharya, "A novel hybrid fusion algorithm to bridge the period of GPS outages using low-cost INS," *Expert Syst. Appl.*, vol. 41, no. 5, pp. 2166–2173, Apr. 2014.
[30] H. O. Sang and D.-H. Hwang, "Low-cost and high performance ultra-tightly coupled GPS/INS integrated navigation method," *Adv. Space Res.*, vol. 60, no. 12, pp. 2691–2706, 2017.
[31] G. Welch and G. Bishop, "An introduction to the Kalman filter," Univ. North Carolina Chapel Hill, Chapel Hill, NC, USA, Tech. Rep., 1995.
[32] T. Fischer and C. Krauss, "Deep learning with long short-term memory networks for financial market predictions," *Eur. J. Oper. Res.*, vol. 270, no. 2, pp. 654–669, 2018.
[33] H. Liu, X. Mi, and Y. Li, "Smart multi-step deep learning model for wind speed forecasting based on variational mode decomposition, singular spectrum analysis, LSTM network and ELM," *Energy Convers. Manage.*, vol. 159, pp. 54–64, Mar. 2018.
[34] G. Rao, W. Huang, Z. Feng, and Q. Cong, "LSTM with sentence representations for document-level sentiment classification," *Neurocomputing*, vol. 308, pp. 49–57, Sep. 2018.
[35] B. Lehner, J. Schlüter, and G. Widmer, "Online, Loudness-invariant vocal detection in mixed music signals," *IEEE/ACM Trans. Audio, Speech, Lang. Process.*, vol. 26, no. 8, pp. 1369–1380, Aug. 2018.

**YUEXIN ZHANG** is currently pursuing the Ph.D. degree with Southeast University, China. She is currently engaged in the research with the Department of Electrical and Computer Engineering, National University of Singapore (NUS), as a joint Ph.D. Student. Her research interests include sensor fusion and intelligence control.